Small- and large-scale characterization and mixing properties in a thermally driven thin liquid film

Michael Winkler[1] and Markus Abel[1,2]
[1]*University of Potsdam, Institute of Physics and Astronomy, 14476 Potsdam, Germany*
[2]*Ambrosys GmbH, 14473 Potsdam, Germany*
(Received 30 July 2015; revised manuscript received 5 October 2015; published 2 December 2015)

We study aqueous, freestanding, thin films stabilized by a surfactant with respect to mixing and dynamical systems properties. With this special setup, a two-dimensional fluid can be realized experimentally. The physics of the system involves a complex interplay of thermal convection and interface and gravitational forces. Methodologically, we characterize the system using two classical dynamical systems properties: Lyapunov exponents and entropies. Our experimental setup produces convection with two stable eddies by applying a temperature gradient in one spot that yields weakly turbulent mixing. From dynamical systems theory, one expects a relation of entropies, Lyapunov exponents, a prediction with little experimental support. We can confirm the corresponding statements experimentally, on different scales using different methods. On the small scale the motion and deformation of fluid filaments of equal size (color imaging velocimetry) are used to compute Lyapunov exponents. On the large scale, entropy is computed by tracking the left-right motion of the center fluid jet at the separatrix between the two convection rolls. We thus combine here dynamical systems methods with a concrete application of mixing in a nanoscale freestanding thin film.

DOI: 10.1103/PhysRevE.92.063002 PACS number(s): 47.55.pb, 05.45.−a, 68.15.+e, 47.51.+a

I. INTRODUCTION

Chaotic or turbulent mixing is essential for many industrial processes, so a profound understanding is essential for practical applications. Despite the fact that basic mechanisms for mixing in dynamical systems [1,2] are well understood, mixing characterization in experiments proves difficult due to more complex conditions and imperfections in real-world implementations. Here the restrictions are finite time, finite length, and complex geometries.

The system under consideration is a freestanding aqueous thin film, which is thermally driven to induce convective motion. The film is almost two dimensional and can show a transient thick phase (several micrometers) and a equilibrium thin phase (∼10–50 nm), both immiscible due to the forces separating them, similar to bubbles (the thin phase) in a three-dimensional liquid phase. Thin liquid films bound to a frame with two free surfaces without contact to a substrate, stabilized by a surfactant, are also known as foam films. Hereafter, we use the term thin film to describe our system.

We have previously examined the thinning behavior of liquid films with focus on an accelerated thinning mechanism by mixing [3]. The thinning speed of the film, i.e., the transition of the whole film to the thin phase, depends primarily on the mixing of thin and thick phases. Without mixing, such a film typically undergoes thinning within several hours; with thermal driving, a flow is established that eventually mixes the phases and leads to a thinning in seconds. Consequently, it is of high interest to understand this mixing and eventually quantify it. In the above-mentioned article, the basic physics are explained. Here we give a quantitative analysis of the mixing properties of the experiment in terms of Lyapunov exponents and entropies. We first discuss briefly the properties of thin liquid films, followed by an explanation of our approach to the characterization of mixing for this highly sophisticated system.

Thin film dynamics is governed by gravitational, capillary, and interfacial forces, where the latter are specified in the disjoining pressure. Combining long- and short-range molecular forces, i.e., electrostatic, van der Waals, and steric forces [4,5], the disjoining pressure depends strongly on the distance between the interacting surfaces. Whereas films on substrates are established in industry and research [6], freestanding thin liquid films still provide a challenge in experiments and theory alike. Consequently, the study of thin films is central to current scientific activities, e.g., [7–12]. We contribute by presenting a way to quantify mixing of vertically oriented, freestanding, thermally forced, nonequilibrium thin films.

As a result of the aforementioned force balance two stable equilibria may occur, depending on the chemical composition of the bulk solution and chosen surface active agents (surfactants): Common black films with a thickness of more than 10 nm are formed when electrostatic interactions balance the dominant van der Waals force and of course gravity and capillarity [4,13] and Newton black films are stable with a thickness of less than 10 nm, due to repulsive short-range steric forces [14,15]. In this study we will focus on films in their transient phase before reaching equilibrium with a typical thickness in the range of 0.1–1 μm. The effect of additional forces has been studied by a several authors, mostly for micrometer-thick systems [16,17].

Quantifying the degree of complexity of an evolving system is a ubiquitous problem in natural science [18]. We will focus on two ways of measuring dynamical complexity: the metric or Kolmogorov-Sinai (KS) entropy h_{KS}, which measures the rate of information production as a fluid particle evolves along a pathline, and the Lyapunov exponents (LEs), which give the rates at which nearby fluid paths diverge [19]. The principle concept of the KS entropy is very natural, as the information contained in the time evolution is a characteristic of the underlying dynamics (cf. Brudno's theorem [20]).

From data one can obtain an estimate by studying the symbolic dynamics acquired by assigning different symbols to different cells of a finite partition of the phase space. The probability distribution of realized sequences (words) is a

signature dynamical evolution. The average information gain is obtained by comparing sequences of lengths m and $m+1$, in the limit of large m: Letting the length of the words m go to infinity and the partition diameter to zero, one obtains the KS entropy, which is often used as a measure of complexity of a system.

Lyapunov exponents λ characterize the exponential divergence of nearby trajectories, typical for chaotic systems [21,22]. One can alternatively state that LEs characterize the sensitivity of a system to initial conditions X_i. They are related to the KS entropy h_{KS} by the Pesin formula

$$h = \sum_{i=1}^{n} \lambda_i > h_{\mathrm{KS}}. \tag{1}$$

Positive Lyapunov exponents indicate that solutions diverge exponentially on average and negative ones indicate convergence. They are computed from time series using embedding techniques [22]; in our case, we can use the spatial information directly and use instead stretching and folding of a fluid area to estimate the local dynamical characteristics directly from the experiment.

II. EXPERIMENT

In this section we describe in detail the experiment, that is, the flow structure that is crucial for the analysis. Then we explain the data analysis we applied, first for the LEs and then for the entropies. In principle, we follow complementary approaches: The LEs are computed from microscopic information, whereas the entropies are determined from the large-scale circulation. Ideally, both quantities should coincide, to be tested by Pesin's formula. We will show the results below.

A. Setup

The experimental setup consists of a vertical rectangular aluminium frame with rounded corners, 45×20 mm^2, enclosed by an atmosphere-preserving cell with a glass window for video recording (see Fig. 1). Thermal forcing is effected by inserting a cooled copper needle (radius 1 mm) at the film center ($T = -169\,^{\circ}$C); the needle enters the cell through a fitting hole. The ambient temperature was constant at 20 °C; the corresponding Rayleigh number Ra $\sim 10^6$, such that the flow is weakly turbulent with a Reynolds number of Re $\simeq 150$.

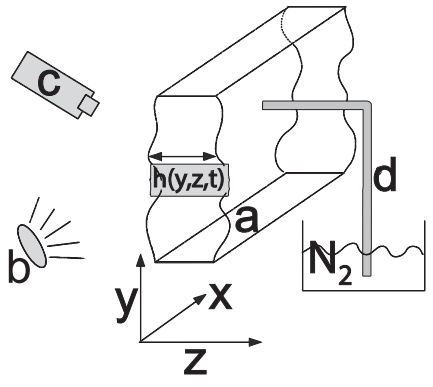

FIG. 1. Setup of the experiment: a, schematic sketch of the free-standing thin film; b, light source; c, camera; and d, cooling rod with liquid nitrogen reservoir.

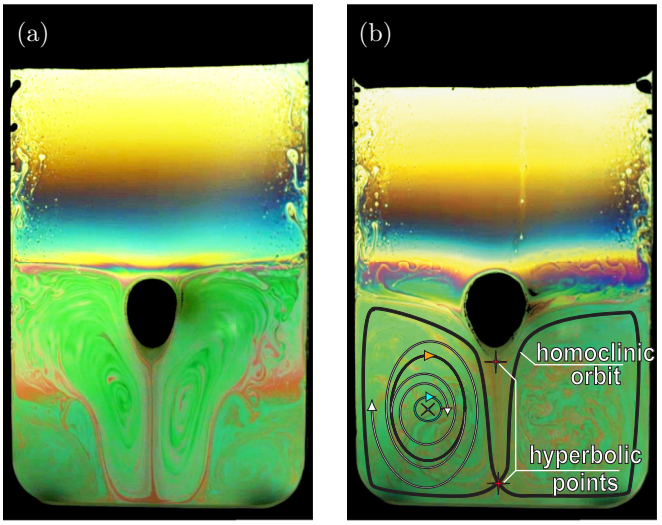

FIG. 2. (Color online) Snapshot of a turbulent convecting thin film. An image of the nonmoving film has been subtracted; the frame and frozen center region including the cooling tip are not shown. On the top, a layer of black film has formed. (a) The convection is not yet fully developed such that corner vortices are observed; they disappear after transients. (b) Weakly turbulent convection has developed. The orbit schematic of the convection is added as an overlay. Orbit schematic: The gray traces represent orbits moving away or towards the center of convection. The elliptic orbits are marked with a light blue circle around the stationary elliptic point (blue cross) in the center of the convection zones. Orange marks the limit between converging and diverging orbits.

Note that for very thin films it is not clear how viscosity changes with the film thickness, since surface forces may matter. We are not aware of any investigations in that direction and will not discuss this further. The given number denotes an order of magnitude such that only dramatic changes in viscosity are relevant, e.g., if the film has a transition to a thin black film and changes structure too. The temperature across the film (in the z direction; see Fig. 1) is approximately constant and the Marangoni number Ma $\simeq 0$. The solution from which the liquid film was drawn consists of the surfactant n-dodecyl-β-maltoside (β-$C_{12}G_2$, $C_\beta = 0.4$ mM), prepared with filtered deionized water and stabilized with 25 vol.% glycerin [23]. The thin liquid film is illuminated with a diffuse broad spectrum light source and its reflection is captured by a high speed camera. Our vertically oriented thin film is produced initially thick (500–5000 nm) by pulling it with a glass rod from the reservoir. Quickly, a wedgelike profile develops with black film in a small region, with a sharp horizontal boundary towards the thick film below (see Fig. 2).

The interference of incident and reflected light yields a striped pattern, which can be used to infer the film thickness. Each color cycle (red to blue) corresponds to multiples n of the smallest negative interference condition $(2n+1)\lambda\eta = 4h\cos\Theta$, where the refraction index η is assumed to be temperature independent and Θ is the angle of incidence [24]. The velocity is measured by color imaging velocimetry [25] with $u \sim 0.02$ m/s.

For ideal two-dimensional (2D) flows, turbulent or not, surface forces are neglected, which also is a reasonable

assumption for experiments with thick (i.e., several micrometers) freestanding liquid films. However, for thin liquid films a complete description involves all occurring forces. A previous time scale analysis for our setup [3] revealed that the dominant driving mechanism is the temperature gradient with Rayleigh number Ra $\sim 10^6$. Other forces can be neglected to first order. The high surface elasticity provided by the surfactant allows the thin film to remain stable in the presence of shear forces (high convection velocities) and thermal fluctuations due to external heating or cooling. This also applies to the equilibrium phase at a thickness below 50 nm.

B. Flow description

This paper presents experimental work and subsequent data analysis, thus we do not discuss the equations of motion of the film, but refer to recent work and reviews for the suitable equations in our situation [5,26,27]. However, we now discuss the observations in order to give the reader an impression of the flow we consider in terms of dynamical systems properties.

We use a point thermal force to drive our system such that we have two rolls, one on each side of the cooling rod (see Fig. 2). The cold rod drives a stable two-eddy convection with a jet of fluid in the center as the driving mechanism and separation at the same time. The deflection of the jet at the lower frame border is sequential and nondeterministic. For the analysis of the large-scale flow, the alternation between the left and the right eddy was visually tracked, recorded during a long time interval and converted into a binary time series as detailed in Sec. II C. Further information on this technique is available in our previous works [3,25,28].

In an abstract way, our flow can be described by geometry (boundary conditions) and four fixed points: The flow is bounded by the enclosing rectangle, which in the upper region is given by the black film region. Boundary conditions are complicated. In the first step they are assumed to be no slip. Then we have the centers of the convection rolls, which are elliptic fixed points. There are two hyperbolic points at the bottom and directly below the lowest part of the ice surrounding the cooling needle and a separatrix running top down, whose connection forms a separatrix [see Fig. 2(b)]. This description holds on short time scales; for long times, we must consider that the whole system is in a transient state, which, however, evolves on much larger time scales such that our considerations are reasonable. A look at corresponding video material will clarify this characterization.

We want to characterize the flow, based on measurements. Key characteristics for mixing and flow in general are stretching or folding of the liquid filaments. We consider respective orbits of fluid elements advected by the two convection rolls, which are stably positioned below the cooling rod. One key question regards the mixing inside the rolls, the other one mixing between the rolls. In contrast to other systems, such as the blinking vortex [1], the vortices are maintained and mixing happens across the separatrix due to small differences in the middle downward flow. Conceptually, we can use the basic ideas of twist maps as one common example for reduce dynamical systems showing mixing. That is, we study the left-right transport, i.e., the mixing between the two rolls.

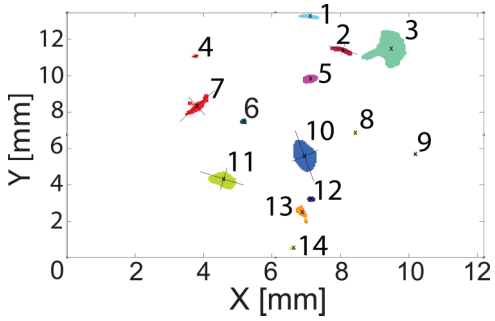

FIG. 3. (Color online) Example of the cluster identification for one frame, including center-of-mass and selected principle components (not to scale).

Below, in Sec. II C, we explain how typical stretching rates are extracted from the experiment, as described in more detail in [25]. We recall the procedure briefly here in order to be complete. Then we analyze in terms of symbolic dynamics in that we analyze the series of liquid transported left and right, i.e., we reduce flow to the fluid exchange between the two rolls. This way we have a local measure by the stretching and a more global one by the transport across the separatrix.

C. Data analysis

The captured video data are postprocessed to enhance colors and contrast. To analyze the behavior of domains of the same thickness the video is converted into a binary image: Fluid filaments of a selected thickness are marked as 1 and the remaining background area is marked as 0.

As the spectrum repeats continually this technique is only valid if the overall thickness deviation is smaller than a full period of the smallest wavelength. Subsequently, in each frame all clusters of the same thickness are numbered and consecutively linked through the following frames (Fig. 3). This enables us to track the volume, velocity, deformation rate, and angular velocity of the moving fluid. For each cluster the velocity is calculated using the shift of its center of mass per frame. The deformation rate is calculated by determining the change of the scale of the principal components per frame. Similarly, the angular velocity is given by the rotation of the principal component. Averaging over all frames then delivers the spatial characteristics of the flow field generated by the cooling tip. The cluster finding algorithm is operating with a linear backward memory of variable depth. However, for now, a tracking of one frame backward is sufficient to maintain connectivity of each cluster through all frames. The memory needs to be limited as merging or dividing clusters would be considered connected, thereby distorting the velocity and deformation rate.

The intermittency of the mixing film is captured by the probability $P(\Delta x, \Delta t)$; we calculate the distance Δx for fixed Δt (on logarithmic scale). The result is plotted in Fig. 4. We observe basically ballistic transport for small Δt, as could be expected because the more chaotic small scales are not resolved and the large-scale transitions are not found by our cluster analysis.

In the generated velocity field (Fig. 5) the fluid is stretched in regions of high velocity and compressed when it enters areas

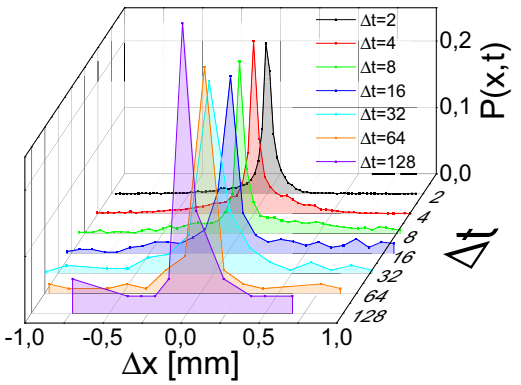

FIG. 4. (Color online) Probability $P(\Delta x, \Delta t)$ for different time scales Δt measured in frames with a frame rate of 100 frames/s. The transport is ballistic over one decade. Larger times are not shown due to the insufficient number of data.

of lower velocity. Due to the shear that is present between layers of different velocity, folding happens. These two processes are the main aspects of mixing in a two-dimensional fluid. Diffusion processes can be neglected as the Reynolds number is of the order of 10^3.

The overall mixing can be characterized within each vortex as an averaging of the stretching rate over the vortex area. The global mixing between the vortices is characterized by the probability of a fluid element to cross the separatrix. This procedure can be seen in the context of effective diffusion, because the averaged turbulent velocity field is a kind of random walker with possibly anomalous and space-dependent transition rates, which when averaged yield the diffusion coefficient. The transition from one cell to the other is the minimal setup, as discussed in [29].

We use a naive approach to analyze our film: Take a spot of material of size Δx, compute its time derivative approximatively from the time evolution as a finite difference, and then use averaging to determine the macroscopic properties. This is in contrast to studies with particles where the velocity of relative dispersion is calculated and is possible only because we have already a field at hand. From the clusters of the same thickness, we obtain the eigenvalues $e^i_{1,2}$ along the principal axes; they correspond directly to the size of the spot numbered i. Averaging the e^i over time and filtering yields an estimate for the fields $e_{1,2}(x,y)$. Now we compare that with the definition of the diffusion coefficient

$$D = \lim_{\Delta t \to 0} \left\langle \frac{[x(t+\Delta t) - x(t)]^2}{\Delta t} \right\rangle.$$

In our situation the limit cannot be reached, due to sampling, and consequently we should use methods like the finite-size LE [30], which is ongoing work. Here we show the results for the finite-size spots with $\Delta t = \Delta_s$ fixed to the minimal sampling time. We make of course an error in mixing different spot sizes, which we counteract by choosing homogeneous spots of similar size.

The space-dependent diffusion is then estimated by

$$D_{\text{est}} = \left\langle \frac{[x(t+\Delta_s t) - x(t)]^2}{\Delta_s} \right\rangle.$$

The average is performed over the number of available frames and all tracked fluid filaments per frame, which sums up to $\sim 10^6$ events. Of course this is a very rough approach, but we will see that in a certain time range we obtain reasonable results and can compare this with the enhancement of thinning. This is not, however, the full story: For mixing it can be desirable to have faster than normal diffusion, the characterization of a real process involves *finite* intervals Δt and Δx, and the degree of anomaly is given by the scaling $\Delta t \sim \Delta x^\alpha$, with $\alpha = 2$ for normal diffusion. Since we prescribe Δt and determine Δx accordingly, the full statistical characterization is given by the probability function $P(\Delta x, \Delta t)$ (see Fig. 4). So we characterize mixing within the two rolls by an effective diffusion approach and the mixing between the two rolls by the statistics of the crossings of the separatrix in the middle of the setup.

The fluid itself offers no contrast to track the motion of filaments. However, the above-described reflection imaging transforms the relative thickness difference of convected filaments into a thickness map whose evolution can be followed and analyzed. Compared to other techniques such as seeding beads or injecting ink, which are unpractical due to the resulting perturbation of the thin liquid layer, the thickness tracking is noninvasive and precise. A drawback (not important here) is that only a relative instead of an absolute thickness map is available and fine layering of filaments is subject to diffusion, thus limiting the resolution.

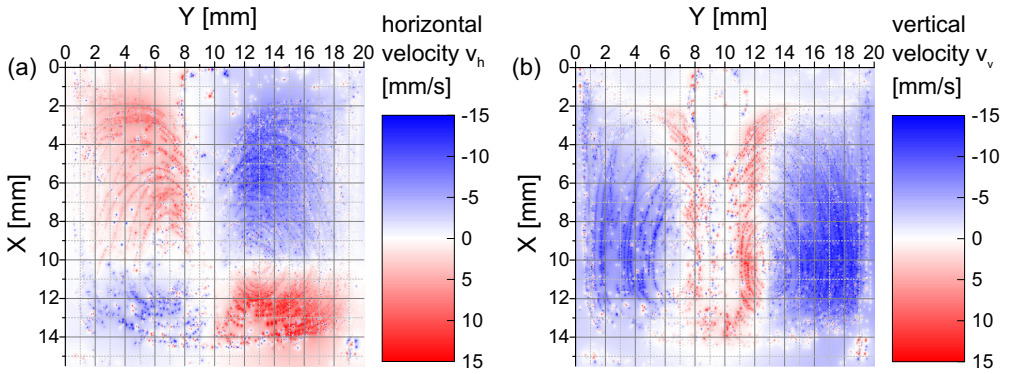

FIG. 5. (Color online) Averaged (a) horizontal and (b) vertical velocity field of the forced advection. The cooling rod is positioned at approximately $p_{\text{rod}}(x,y) = [2\text{ mm}, 10\text{ mm}]$.

In this study we investigate as well the center stream in between the two stable vortices, which is deflected either to the right or to the left at the bottom of the frame. At the cooling rod fluid from both vortices is formed into a center stream. As the convection is bound by the frame, the center jet is deflected sequentially to the left or to the right at the bottom hyperbolic point. This gives a relative measure of the amount of fluid mixed macroscopically between the left and right eddy. The binary series of transports can then be used to estimate the efficiency of this mechanism by calculating the entropy and stochastic properties.

III. METHODS AND RESULTS

In this section we present methods and results based on the data obtained as described above. Section III A treats Lyapunov exponents, estimated by the stretching and folding of small fluid elements. In this sense we only find finite-size values, which characterize the small-scale properties of the flow (and not the infinitesimal ones, as one would need for the true Lyapunov exponents). Within that section we briefly recall and comment on the relation of measures from mixing theory and dynamical systems. In Sec. III B results on the estimation of entropies are shown. We estimate the characteristic entropies by the symbolic dynamics approach [22,29] forming words of a certain length, compute their frequencies as estimators of the probabilities, and eventually obtain an estimate for the entropy production with increasing word length. At the end of this section we compare both measures using known relations.

A. Lyapunov exponents

In dynamical systems theory, LEs are key quantities for the characterization of systems. An equivalent is the efficiency in mixing theory for fluids. Essentially, in a fluid, the stretch of a fluid filament is important, analogous to the stretching of a phase space element in a dynamical system. In our case, both quantities are identical. Furthermore, the mixing efficiency is nothing but a normalized version of the Lyapunov exponent for an ergodic system, since the time and ensemble average need to coincide for the equivalence to hold.

In the following we describe how to estimate mixing efficiency and LEs λ starting from the stretch s of a fluid filament along its trajectory, where

$$s = \lim_{\Delta x_0 \to 0} \frac{\Delta x_t}{\Delta x_0} \tag{2}$$

for the fluid velocity measured in the Eulerian (i.e., laboratory) frame. Here Δx_0 denotes the initial separation of two fluid points at time $t = 0$ and Δx_t the corresponding separation at time t. To satisfy the limit towards elements Δx_0 of infinitesimal length, the cluster data are filtered to contain only the smallest clusters available. The local stretching rate $\frac{ds}{dt}$ (see Fig. 6) is measured in a moving reference system (Lagrangian); therefore the velocity of the separating edges of a fluid filament are observed.

The Lyapunov exponents λ describe the typical property of chaotic systems, in particular 2D systems with hyperbolic points: The trajectories of two nearby points diverge

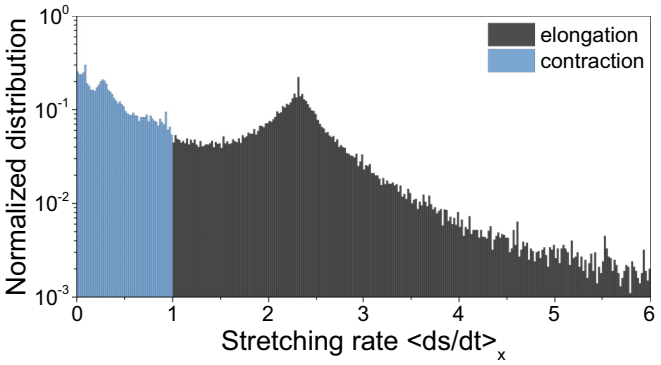

FIG. 6. (Color online) Semilogarithmic plot of the spatially averaged stretching distribution. For better visibility stretching and contracting rates are displayed in contrasting color. The main difference lies in the behavior for contracting values, which can be zero, i.e., the spot observed vanishes. This is reminiscent of our data analysis (explained above) and is not expected for a perfect measurement.

exponentially. We can relate that to fluid motion (for details see, e.g., [21,31]). The exponential divergence for infinitesimally small times is expressed as $\Delta x_t \sim \Delta x_0 e^{\lambda t}$. The local Lyapunov exponent is then given as the long time average of the logarithmic stretching rate (see Fig. 7)

$$\epsilon_s = \frac{D \ln s}{Dt} \to \lambda_l = \lim_{t\to\infty} \frac{1}{t} \int_0^t \epsilon_s dt', \tag{3}$$

where we recognize the difference from the stretch (2) in averaging the logarithm or the ratio of the lengths directly. For ergodic systems, the time and (phase) space average are identical and we can compute alternatively

$$\langle \lambda \rangle_{x,t} = \Big\langle \lim_{\Delta x_0 \to 0} \lambda_l \Big\rangle_x, \tag{4}$$

with the notation $\langle\,\rangle_x$ for the space average. We can compute the two Lyapunov exponents from the contraction $(-)$ and elongation $(+)$ of the tracked fluid filaments and obtain as an estimate of the overall mixing properties of the flow

$$\langle \lambda_- \rangle_{x,t} = -1.43, \quad \langle \lambda_+ \rangle_{x,t} = 0.92. \tag{5}$$

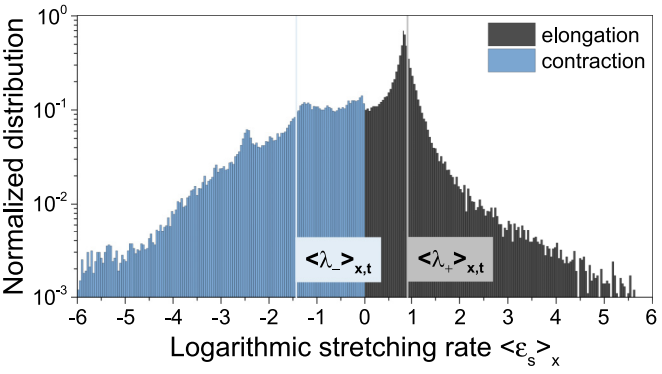

FIG. 7. (Color online) Distribution of the stretching rate ϵ_s. The average over time gives the Lyapunov exponents $\langle \lambda_- \rangle_{x,t} = -1.43$ and $\langle \lambda_+ \rangle_{x,t} = 0.92$, indicated by the vertical lines. Clearly, the distribution of negative and positive LEs is different.

If the flow is conservative $\|\lambda_-\lambda_+ = 1\|$, here we find a contraction considerably smaller than $-1/0.92 \simeq -1.087$. It is explained by the fact that we measure not only the stretch, but in addition the general volume loss of a spot of a certain color due to film thinning and diffusion of the thickness map, as explained above (see Fig. 3); this contributes to the negative LE.

The distributions of the positive and negative LEs are quite different. This is explained by the dynamics: Elongation (the positive LE) takes place mainly in the rapid flow region between the two fixed points (the separatrix). This leads to a very pointed distribution with faster than exponential decay (see Fig. 7, dark gray part). In contrast to this, contraction happens over the whole region of the film with quite different and much slower dynamics. Additionally, the contraction rate data have a lower signal to noise ratio compared to the elongation rate, as the absolute values are smaller and closer to the resolution limit of the setup.

Before discussing the estimation of the entropy we describe the connection between the LE and mixing efficiency. Both quantities are closely related:

$$\langle E_s \rangle = \frac{1}{t}\int_0^t \frac{\epsilon_s}{\sqrt{\vec{D}\otimes\vec{D}}}dt'. \tag{6}$$

We see that the difference lies in the normalization. It involves the symmetric part of the velocity gradient $\vec{D} = \frac{1}{2}[\vec{\nabla}\vec{v} + (\vec{\nabla}\vec{v})^T]$ (equivalent to the stretching tensor), where $\vec{D}\otimes\vec{D}$ needs to be constant over the pathlines for this expression to be valid. It is used as a normalization to obtain a stretching efficiency smaller than or equal to one. Using this normalization, one can demonstrate [1] that the upper bound of the efficiency for two-dimensional flows is $E_{s,\max} = \sqrt{2}/2 = 0.707$ [1]. Since the stretching tensor is not readily available from the cluster data and is only used as a normalization in Eq. (6) it was not used here and we refer to the unnormalized Lyapunov exponents.

B. Entropy

Similar to the Lyapunov exponent, the entropy production of a dynamical system is a measure of its chaoticity. Here we compute the Kolmogorov-Sinai entropy h_{KS} for the center jet deflection and compare it to $\langle\lambda_{-/+}\rangle_{x,t}$, which we obtain from the stretching rates of the fluid filaments. The topological entropy h is the upper limit for the average Lyapunov exponent $h \geqslant \langle\lambda\rangle$ [31] and the Pesin formula equates the topological entropy with the sum of all positive Lyapunov exponents $h = \sum_{i=1}^{n}\lambda_{+,i} > h_{\mathrm{KS}}$ and sets the limit for h_{KS} [32]. More precisely, the relation between the topological entropy h and h_{KS} is given via the variational principle $h(T) = \sup[h(\mu)_{\mathrm{KS}} : \mu \in \mathcal{P}_T(X)]$, where μ ranges over all T-invariant Borel probability measures on X. Thus h is an upper limit for the KS entropy. A direct relation between Lyapunov exponents and entropy is available via the information dimension

$$D_I = h(\mu)\left(\frac{1}{\langle\lambda_+\rangle_{x,t}} + \frac{1}{|\langle\lambda_-\rangle_{x,t}|}\right) \tag{7}$$

of an ergodic invariant measure μ of a smooth invertible map with Lyapunov exponents $\langle\lambda_+\rangle_{x,t} > 0 > \langle\lambda_-\rangle_{x,t}$ [21,33]. Here $\langle\lambda_+\rangle_{x,t}$ and $\langle\lambda_-\rangle_{x,t}$ denote Lyapunov exponents calculated from stretching (+) and contraction (−) rates, respectively. Comparing Eq. (7) to the Kaplan-Yorke conjecture [34] $D_L = 1 + \langle\lambda_+\rangle_{x,t}/|\langle\lambda_-\rangle_{x,t}|$, with Lyapunov dimension D_L, suggests that $h(\mu) = \langle\lambda_+\rangle_{x,t}$ in the case of the natural measure of a 2D smooth invertible map.

Let us now compute the values for the entropy to the degree our data allow with respect to the length of the time series and accuracy. First, we need to define a kind of alphabet to identify words. Our procedure follows essentially [29] and for more details we refer to that work. The jet is deflected into either the left or the right vortex at the bottom of the frame. We analyze the deflection pattern to check for systematic effects (e.g., tilting of the device), which would lower the mixing efficiency of this fluid transport.

The sequence of left (treated as 0) and right (treated as 1) transports is a binary time series from which one can associate a word of length n, out of a finite alphabet: $W_k^n = (S_k, S_{k+1}, \ldots, S_{k+n-1})$. The block entropies H_n are then calculated from the word probability distributions $P(W^n)$:

$$H_n = -\sum_{W^n} P(W^n)\ln P(W^n), \tag{8}$$

where W^n represents the set of all possible words of length n. The entropy per unit time is defined as

$$\begin{aligned} h_n &= H_{n+1} - H_n, \\ h_{\mathrm{KS}} &= \lim_{n\to\infty} h_n. \end{aligned} \tag{9}$$

In the presented case the practical limit of h_{KS} is given by the finite series of events thus truncating the number of possible words and the possible entropy gain by increasing the word length. Here h_n can be interpreted as the rate of information production, which for a finite signal decreases when the combined length of all possible words W^n becomes longer than the signal itself: $\sum_{W^n} n > l_S$. The mixing efficiency is maximal when the jet deflection is uniformly distributed for left and right. Therefore, we use a set of uniform left-right probability as a benchmark for the measurement data. As expected, the entropy h_n remains constant with increasing word length until the finite-size limit of the data set is reached; longer sets hit this limit at longer word lengths (see Fig. 8).

The entropy h_n of the different distributions below this limit is identical, in particular for the data with the same length as the measurement set. Therefore, the deviation in h_n of the measurement data when compared to the uniformly distributed data sets cannot simply be omitted as a finite-size effect. The h_n of the measurement data is approximately 15%–20% below the possible maximum given by the random sequences, which indicates a nonuniform process or deterministic behavior [see Fig. 8(b)].

One might assume that the sequence is tilted towards one side and that this preference causes the flow pattern to be more predictive. To check for this property we compared the data set to skewed random distributions, which have a lower entropy production due to the higher predictability of the signal. In Fig. 9 random sets with an uneven distribution up to a probability of $P = 0.9$ for one direction of the flow are compared. The entropy production of a 77/23-skewed distribution is comparable to the measurement data. In this case

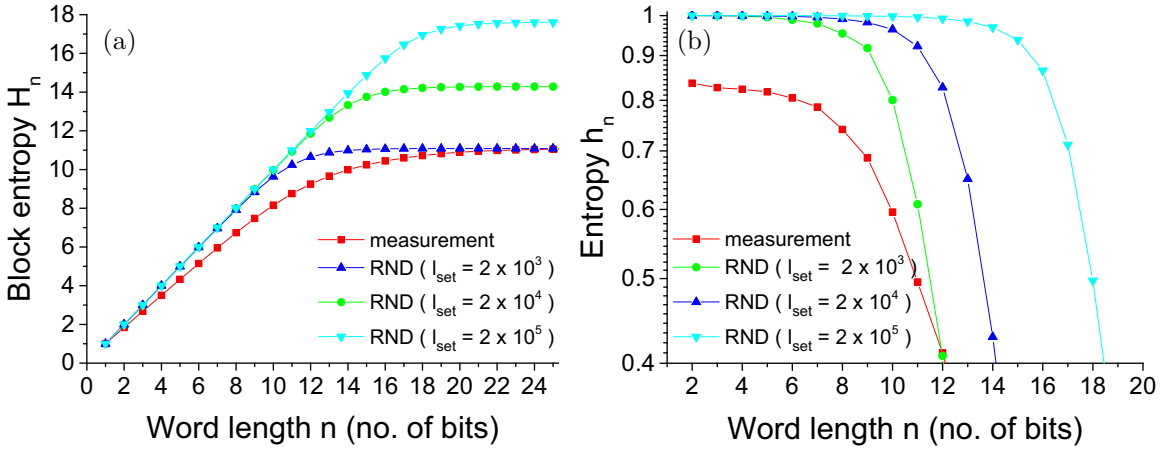

FIG. 8. (Color online) (a) Block entropy H_n and (b) entropy h_n with increasing word length of the measurement set (set length 2×10^3), compared to random distributions (RND) of variable set length l_{set}.

the deflection of the center jet would be directed towards one side approximately 8 out of 10 times. However, the distribution of left and right transports in the measurement data is even, which shows that the deterministic components of the signal is not due to a simple asymmetry in the experimental setup.

Conditional probabilities. Another option to check for deterministic components is to look for recurrent sequences in the signal. Therefore, we calculate the conditional probabilities $P(W^n|W^m)$ with $n = m = 1, \ldots, 4$ to look for recurring patterns with a memory of up to 4. This limit applies due to the finite data set size; therefore, the total word length $l_W = n + m$ for our measurement is restricted to 8. For each word length the conditional probabilities of all possible combinations are calculated giving a matrix of size $n \times n$. Again we compare to a random signal of the same size as the measurement data set. For a random data set of infinite length one expects an even distribution of conditional probabilities. However, as we compare finite-size data sets, the conditional probabilities become nonuniform at longer word lengths as not all combinations are represented equally [see Fig. 10(b)]. The figure displays the deviation from a perfect random distribution, which would show as a 50% gray tile.

The conditional probabilities of the data set deviate substantially from the even distribution the random data provide [see Fig. 10(a)]. The jet is more likely to alternate between left and right transports, which is evident by the higher conditional probabilities of alternating binary combinations, i.e., $P(W^n|1010), P(W^n|0101)$. Some combinations with two or more consecutive transfers in the same direction show a higher than average probability, but these are always combined with alternating sequences. Uniform combinations, i.e., $P(W^n|0000), P(W^n|1111)$, are extremely rare events.

The diminished entropy production with increasing word length is caused by a preference for alternating transfers, which are evidenced by nonuniform conditional probabilities. The signal is more predictable and most common combinations are already covered with shorter length words, thus the additional words carry less new information.

Eventually, we compare the results from the entropy and LE estimation. For the LE we obtained $\lambda_+ = 0.92$ and $\lambda_- = -1.43$. For the Shannon entropy we can read off the entropy gain from Fig. 9 (red line and markers) as $h_{\text{KS}} = 0.82$. Using the Kaplan-Yorke conjecture, we should find a coincidence $h \simeq \langle \lambda_+ \rangle$ with a Kaplan-Yorke dimension of 1.92. Given the

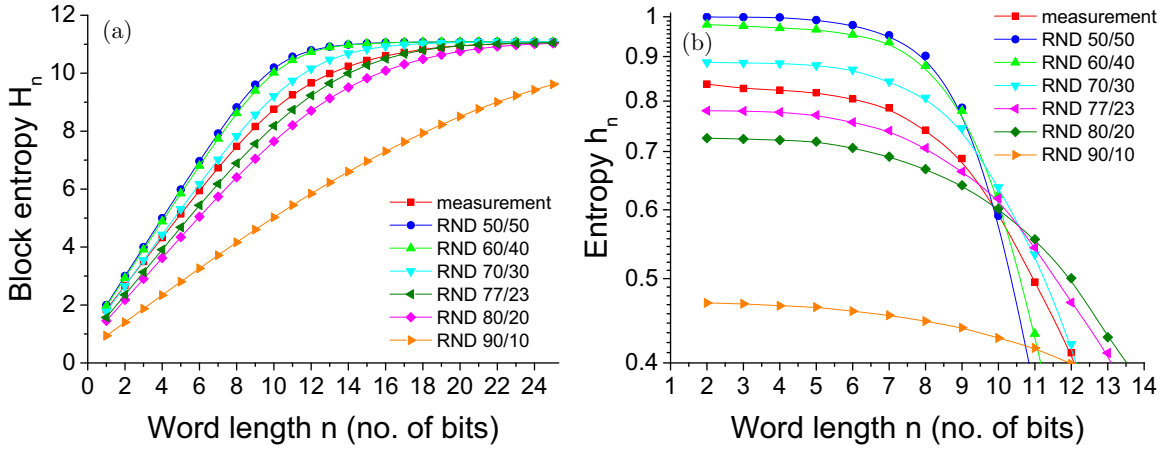

FIG. 9. (Color online) (a) Block entropy H_n and (b) entropy h_n of the measurement data compared to random distributions (RND) with varying skewness. The skewness is given as the ratio of left versus right transports. The data set length is constant.

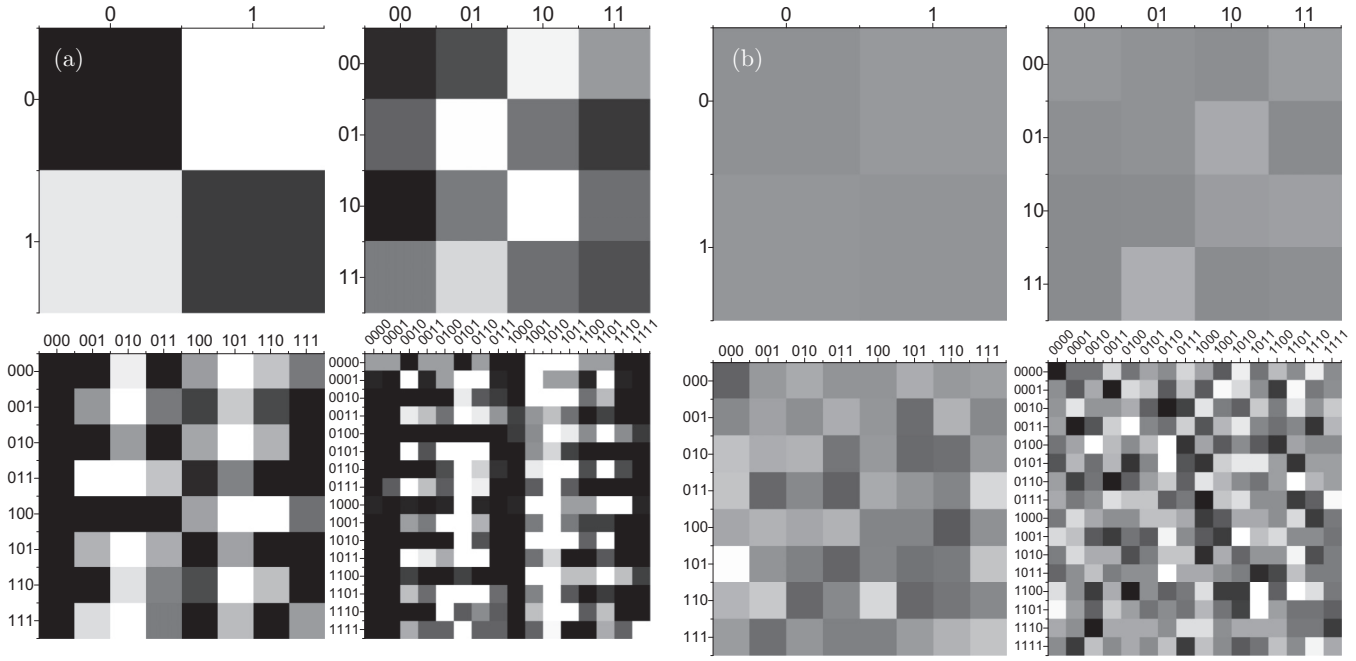

FIG. 10. (a) Conditional probabilities for measurement data compared to (b) a random distribution. Each tile represents the conditional probability $P(W^m|W^n)$, where W^m is plotted on the x axis and W^n is plotted on the y axis. The word length $l_W = 1, \ldots, 4$. The grayscale for each plot is centered at the expected probability, i.e., for $l_W = 2$: $P(W^m|W^n) = 0.25$ for all possible combinations. From this value the scale covers 50% deviation, i.e., $l_W = 2$: black, $P(W^m|W^n) = 0.125$; white, $P(W^m|W^n) = 0.375$.

error sources in the LE estimation and the relatively short time series, we consider this result a very good coincidence.

IV. DISCUSSION AND SUMMARY

We presented a relatively simple experiment exhibiting complex dynamics, where weakly turbulent mixing reaches down to the nanoscale, at least in one dimension. This renders the flow two dimensional, however with additional forces acting between the surfaces: disjoining pressure and capillary pressure.

With respect to turbulence, we observed that the relatively-low-Ra convection generates a weakly turbulent flow with two prominent rolls. The turbulence mainly can be observed inside the rolls on shorter time scales, whereas transport between the rolls is on a slow scale and shows signs of chaos. To characterize the flow, we took advantage of our measurement capacities and the color imaging velocimetry (CIV) technique. In addition to the flow field, concluded from Lagrangian trajectories, we obtained local deformation rates that are used to estimate the Lyapunov exponents. With respect to mixing, we clearly observed the typical chaotic filamentation. As mentioned in the context of weak turbulence, global mixing on the large scale happens between the left and right convection rolls.

We focused on two different methods to quantify the dynamics of the flow: Lyapunov exponents and entropies. Whereas the LEs are calculated using small-scale dynamics using CIV, i.e., tracking of small fluid spots, entropies have been calculated using the left-right transport across the separatrix. Qualitatively, these two observations are related by the two spots generating the dynamics: the hyperbolic fixed points. They determine the microscopic properties (LEs) and the transport across the separatrix. Thus, based on dynamical systems principles, one expects that both quantities coincide. Given the two different approaches and the very different spatial scales, this coincidence is a formidable confirmation of theory. For the given experimental setup, temperature could not be controlled, which limits the generality of our results. A setup with temperature control is currently built such that one can verify the results using the improved configuration.

The presented data were gathered from eight individual runs of the experiment. Entropy production and conditional probabilities were calculated for the data set and compared to truly random data sets of varying size and skewness. The conditional probabilities show that an alternating pattern of left and right transports is preferred, which increases the predictability and lowers the entropy production of the measurement data with respect to uniformly distributed data. The number of left and right transports in the data is even with a deviation of 2% from the exact left-right randomly uniform distribution, which can be accredited to inaccuracy of experimentally obtained data (rod not positioned at the exact center) and limited data set length. Although the entropy production h_n is comparable to a skewed random distribution with an approximately 70/30 shift, these are two unlinked deterministic mechanisms that lead to a decrease of h_n.

Due to the shortness of the time series, an entropic analysis has errors beyond a certain length of the words formed. In order to have a quantitative measure for this length we compared the measurement with numerically determined left-right random sequences without memory. As displayed by the random data sets of varying size, a larger data set would yield

higher accuracy in the entropy production rate and conditional probabilities, but the fundamental scaling behavior remains the same. Thus the statistical evaluation of the measurement data is valid.

Using such a numerical validation procedure, we found clearly that the asymmetry found should be attributed to higher-order memory in the data. This is quite plausible, since we are investigating a fluid system, where memory is built in for advected particles and so for advected fluid particles too. The calculated KS entropy serves as an upper limit to the Lyapunov exponents, which were calculated from the stretching rates. Experimentally, we used color tracking, which focuses on small scales. This area tracking algorithm provides detailed information about the flow field and is adaptable to work on any data of deformable clusters with high enough contrast with respect to their surrounding.

One key question regards the consistency of the LE and entropy estimates. We found astonishingly close results for the entropy and LE using the Kaplan-Yorke conjecture. Both agreed within an error of 10%. The values of 0.92 and -1.43 indicate a relatively moderate large-scale mixing, which is due to the fact that the setup involves only two main flow regions in which one has to achieve mixing.

However, in practical terms, such nanofluidic devices can be well used as free-standing mixers with very flexible surface properties. The mixing times are then quite fast, since the device dimensions can be miniaturized further. The true advantage lies in the very good ratio of the surface and volume of the film: Such a film has an enormous surface; in our setup the ratio was $1{:}10^5$, which is probably only achievable with thin films. The free-standing property, finally, allows us to avoid problems with solid-liquid interface forces; rather, one can focus on a chemically favorite design of the equally treated surfaces.

Generally, we think that with our relatively simple experiment we can answer deep physical questions on the microscopic nature of thin film flows and treat at the same time very practice-oriented topics.

[1] J. M. Ottino, *The Kinematics of Mixing* (Cambridge University Press, Cambridge, 1989).

[2] C. R. Doering and J. D. Gibbon, *Applied Analysis of the Navier-Stokes Equations* (Cambridge University Press, Cambridge, 1995), Vol. 12.

[3] M. Winkler, G. Kofod, R. Krastev, S. Stöckle, and M. Abel, Exponentially Fast Thinning of Nanoscale Films by Turbulent Mixing, Phys. Rev. Lett. **110**, 094501 (2013).

[4] B. V. Derjaguin, *Theory of Stability of Colloids and Thin Films* (Consultants Bureau, New York, 1989).

[5] A. Oron, S. H. Davis, and S. G. Bankoff, Long-scale evolution of thin liquid films, Rev. Mod. Phys. **69**, 931 (1997).

[6] G. Reiter, The artistic side of intermolecular forces, Science **282**, 888 (1998).

[7] H. Kellay, Turbulence: Thick puddle made thin, Nat. Phys. **7**, 279 (2011).

[8] P. J. Yunker, T. Still, M. A. Lohr, and A. G. Yodh, Suppression of the coffee-ring effect by shape-dependent capillary interactions, Nature (London) **476**, 308 (2011).

[9] T. Kanyanee, J. Jakmunee, K. Grudpan, and P. K. Dasgupta, Doped soap membranes selectively permeate a chiral isomer, J. Am. Chem. Soc. **132**, 18045 (2010).

[10] Henning Krusemann, Lattice Boltzmann Simulation of 2D Thermal Convection, Institute of Physics and Astronomy, Potsdam University, Germany, 2012.

[11] D. Exerowa and P. M. Kruglyakov, *Foam and Foam Films: Theory, Experiment, Application* (Elsevier, New York, 1998).

[12] J. Vermant, Fluid mechanics: When shape matters, Nature (London) **476**, 286 (2011).

[13] E. J. W. Verwey and J. T. G. Overbeek, *The Theory of the Stability of Lipophobic Colloids* (Elsevier, Amsterdam, 1948).

[14] M. N. Jones, K. J. Mysels, and P. C. Scholten, Stability and some properties of the second black film, Trans. Faraday Soc. **62**, 1336 (1966).

[15] J. N. Israelachvili, *Intermolecular and Surface Forces* (Academic, London, 1991).

[16] J. Zhang and X. L. Wu, Velocity Intermittency in a Buoyancy Subrange in a Two-dimensional Soap Film Convection Experiment, Phys. Rev. Lett. **94**, 234501 (2005).

[17] F. Seychelles, Y. Amarouchene, M. Bessafi, and H. Kellay, Thermal Convection and Emergence of Isolated Vortices in Soap Bubbles, Phys. Rev. Lett. **100**, 144501 (2008).

[18] R. Badii and A. Politi, *Complexity Hierarchical Structures and Scaling in Physics* (Cambridge University Press, Cambridge, 1997).

[19] A. J. Lichtenberg and M. A. Lieberman, *Regular and Chaotic Dynamics* (Springer, Berlin, 1992).

[20] R. W. Batterman and H. White, Chaos and algorithmic complexity, Found. Phys. **26**, 307 (1996).

[21] E. Ott, *Chaos in Dynamical Systems* (Cambridge University Press, Cambridge, 2002).

[22] H. Kantz and T. Schreiber, *Nonlinear Time Series Analysis* (Cambridge University Press, Cambridge, 2004), Vol. 7.

[23] S. Stöckle, P. Blecua, H. Möhwald, and R. Krastev, Dynamics of thinning of foam films stabilized by n-dodecyl-β-maltoside, Langmuir **26**, 4974 (2010).

[24] L. J. Atkins and R. C. Elliott, Investigating thin film interference with a digital camera, Am. J. Phys. **78**, 1248 (2010).

[25] M. Winkler and M. Abel, Mixing in thermal convection of very thin free-standing films, Phys. Scr. **T155**, 014020 (2013).

[26] H. Krusemann (unpublished).

[27] T. Erneux and S. H. Davis, Nonlinear rupture of free films, Phys. Fluids A **5**, 1117 (1993).

[28] M. Winkler and M. Abel, Droplet coalescence in 2d thermal convection of a thin film, J. Phys.: Conf. Ser. **333**, 012018, (2011).

[29] M. Abel, L. Biferale, M. Cencini, M. Falcioni, D. Vergni, and A. Vulpiani, Exit-time Approach to ε-entropy, Phys. Rev. Lett. **84**, 6002 (2000).

[30] E. Aurell, G. Boffetta, A. Crisanti, G. Paladin, and A. Vulpiani, Growth of Non-infinitesimal Perturbations in Turbulence, Phys. Rev. Lett. **77**, 1262 (1996).

[31] T. Tél and M. Gruiz, *Chaotic Dynamics: An Introduction Based on Classical Mechanics* (Cambridge University Press, Cambridge, 2006).

[32] D. Ruelle, *Chaotic Evolution and Strange Attractors* (Cambridge University Press, Cambridge, 1989), Vol. 1.

[33] L.-S. Young, Dimension, entropy and Lyapunov exponents, ergodic theory and dynamical systems, Ergod. Theory Dyn. Syst. **2**, 109 (1982).

[34] P. Frederickson, J. L. Kaplan, E. D. Yorke, and J. A. Yorke, The Liapunov dimension of strange attractors, J. Differ. Equations **49**, 185 (1983).